Finite Element Simulations of Tip-Enhanced Raman and Fluorescence Spectroscopy

Andrew Downes,*,† Donald Salter,‡ and Alistair Elfick†

Institute of Materials and Processes, University of Edinburgh, King's Buildings, Mayfield Road, Edinburgh EH9 3JL, United Kingdom, and The Queen's Medical Research Institute, University of Edinburgh, 47 Little France Crescent, Edinburgh EH16 4TJ, United Kingdom

Received: January 10, 2006; In Final Form: February 13, 2006

Finite element electromagnetic simulations of scanning probe microscopy tips and substrates are presented. The enhancement of the scattered light intensity is found to be as high as 10^{12} for a 20 nm radius gold tip, and tip−substrate separation of 1 nm. Molecular resolution imaging (<1 nm) is achievable, even with a relatively large radius tip (20 nm). We also make predictions for imaging in aqueous environments, noting a sizable red shift of the spectral peaks. Finally, we discuss signal levels, and predict that high-speed Raman mapping should be possible with gold substrates and a small tip−substrate separation (<4 nm).

Introduction

Scanning probe microscopy (SPM) is an extremely powerful tool for nanoscale characterization of surfaces, indeed it is capable of atomic resolution. However, chemical information about the surface is not normally available.[1] Optical microscopy, on the other hand, is capable of chemical and structural analysis—especially with Raman spectroscopy—but is limited in resolution by the wavelength of light to around 200 nm. Combining the benefits of the two techniques has the potential to create the ultimate nanoscale analytical tool for the measurement of physical and chemical properties.

The first near-field optical probes were made from drawn optical fibers.[2] The resolution of this technique is limited by the size of the aperture milled out of a metal coating by a focused ion beam. More recently, light has been scattered from the region around the apex of sharper metal tips in so-called 'apertureless' near-field optical microscopy.[3,4] The tip acts like an antenna, enhancing the optical field directly beneath the tip by orders of magnitude.[5] Raman spectroscopy is also achievable on the nanoscale.[5−8] Here, photons lose some energy in exciting molecular vibrations, the re-emitted photons being red-shifted and containing information about the region under the tip. Tip-enhanced Raman spectroscopy (TERS) offers the hope of characterizing individual molecules and the smallest of nanoscale objects.

Raman spectroscopy is the ultimate method of optical characterization, giving chemical information from the position of sharp peaks in the spectrum of scattered light and giving structural information from the shift of peaks from their normal position. Raman cross-sections are typically very low (10^{-30} cm^2),[9] so spectral acquisition is relatively slow—a useful spectrum can be acquired in about 1 s in far-field systems. A TERS enhancement of 6×10^6 has been reported for a molecule between a gold tip and flat gold substrate.[5] Gold-coated atomic force microscope tips can be used,[8] but this tends to increase the end radius to 30−50 nm. Alternatively etched wires can be employed for shear force[6,10] or scanning tunneling microscopy (STM) feedback;[5] gold wires can be etched down to radii of approximately 20 nm. Even higher enhancements have been recorded for surface-enhanced Raman spectroscopy (SERS) for dye molecules between colloidal particles. Nie and Emory[11] and Kneipp et al.[12] have reported values of 10^{12}−10^{14}. Tip-enhanced fluorescence has also been reported with 10 nm resolution[13] but the fluorophore must not be too close to the gold substrate or fluorescence will be quenched.

Several studies have modeled optical scattering from the isolated tip apex region,[14,15] but few have included the influence of the substrate.[16−19] Despite these models, the influence of many parameters remains uncertain; so in this article we consider realistic tips, substrates, and scanning conditions, with particular regard to the Raman process.

The aim of this article is to employ a previously used finite element model[18] to calculate the optical enhancement as a function of wavelength or Raman shift, for a variety of conditions. Atomically flat surfaces of gold, mica, and silicon will be considered as substrates; these materials being commonly used as SPM substrates. The variation of the enhancement with spatial position beneath the tip and laterally across the substrate will be calculated. Aqueous environments will be modeled for the first time, to compare with findings for scanning in air. The direction and polarization of excitation laser will also be investigated to find the optimum conditions for illumination. Subsequently, we will discuss the implications of the results especially in terms of signal levels and resolution for Raman mapping and spectroscopy of a film of hydrocarbon molecules on flat substrates.

Methods

Finite element models were created with ANSYS Multiphysics software with a high-frequency electromagnetic option. Maxwell's equations are solved across a defined region containing the tip, substrate, and air or water gap. The geometric model is split into 10^5 small elements, the size of which varies across the model down to about 0.5 nm in the end of the tip, gap, and top layer of substrate just beneath the tip. The tip consists of a hemisphere of radius (normally) 20 nm, placed at the end of a cone of half angle 10°. This represents a tip radius achievable by electrochemical etching in hydrochloric acid.[20] The boundary

* To whom correspondence should be addressed. E-mail: andy.downes@ed.ac.uk.
† Institute of Materials and Processes.
‡ The Queen's Medical Research Institute.

10.1021/jp060173w CCC: $33.50
Published on Web 03/16/2006

condition applied to the exterior of the model is $Z = \mu_0/\epsilon_0$, μ_0 and ϵ_0 being the permeability and permittivity of free space. A p-polarized plane wave is applied, normally incident from 45° (between the tip axis and substrate plane), whose amplitude is set to 1. The calculated value of electric field amplitude in the tip apex region is thus equal to the enhancement of the incident electric field amplitude, E_{elec}.

Scattering from the tip region is a two-stage process. First, the tip region must be excited, then the region radiates. The overall enhancement of the scattered light intensity, E_{scat}, is given by the product of the incident electric field intensity enhancement and the radiated electric field intensity enhancement, $(E_{elec}(\lambda_{inc}))^2 \cdot (E_{elec}(\lambda_{rad}))^2$, λ_{inc} and λ_{rad} being the incident and radiated wavelengths, respectively. The incident and radiative processes are symmetric, being equal when the incident and radiated wavelengths are equal (i.e. no losses), so the intensity enhancement $E_{scat} = (E_{elec}(\lambda_{inc}))^4$ in this case.

For Raman spectroscopy in the visible range, the radiated wavelength can be longer than the incident wavelength by about 100 nm—a similar figure to that of the fluorescence process—so we need a broad response curve for E_{elec}. Silver tips have been shown to possess resonances as sharp as 5 nm[18] so are considered inappropriate for Raman or fluorescence studies. This is in contrast to SERS experiments which involve larger (~100 nm) silver spheres, where the resonance is red-shifted and far broader. Such large radii will not produce high-resolution images in either topographic or optical images. Instead, gold is the preferred metal, and its lack of oxidation makes it a good candidate for practical microscopy.

We used experimentally determined complex optical constants for gold and silicon,[21] and constant refractive indices for mica (1.58), water (1.33), and saturated hydrocarbons (1.46) were used. These were fed into the ANSYS simulations for a given wavelength.

Results

Imaging in Air. The enhancement of the electric field is calculated across the whole model, for a given direction of incidence and polarization of radiation. In-plane (p-polarized) light gives a much higher enhancement than out-of-plane polarization (s-polarized), as the electric field has a component in the axis defined by the direction of the length of the tip. This gives rise to a larger vertical dipole, hence a higher rate of re-radiation.

This is demonstrated by the simulation in Figure 1, for a gold tip of radius 20 nm positioned 2 nm above a mica surface. Light of wavelength 533 nm is incident at 45° to the tip axis, representing illumination with a long working distance lens. In reality, the region will be illuminated with a range of angles. All data presented in this article have p-polarization incident at 45°, unless otherwise stated.

A gold tip and substrate are modeled as a function of wavelength in Figure 2a, for a variety of tip−substrate separations. Simulations were performed at intervals of 0.1 eV, with the addition of a point at 533 nm for our laser. The enhancement of scattered light intensity is plotted as the fourth power of the electric field enhancement, i.e. for $\lambda_{inc} = \lambda_{rad}$. The peak shifts very slightly from 533 to 539 nm as the separation decreases. This red shift is also seen in models of photon emission from the scanning tunneling microscope.[22,23] The calculated energies of localized plasmon modes decrease in energy (hence increase in wavelength) as separation decreases, or equivalently as tip radius increases. The gold tip can support a plasmon on its own, but when a substrate is brought into close proximity a localized plasmon is present in the end of the tip, substrate, and gap. A mica substrate is relatively passive, but an image of the tip is formed within the substrate (in order to maintain electric field and displacement field boundary conditions across the surface). This gives rise to a larger vertical dipole than for an isolated tip. A gold surface supports a larger dipole than a mica surface thanks to its larger real part of the dielectric function. The response curve is quenched for wavelengths below about 490 nm or at energies above where the real part of the dielectric function of gold is equal to −2. Above this energy, the localized plasmon extended over the tip, gap, and substrate is quenched by preferentially exciting a spherical plasmon in the end of the tip. This spherical plasmon occurs when the dielectric function is −2, which is akin to quenching by surface plasmons for a dielectric function of −1 or by volume plasmons for 0. This spherical plasmon has a much smaller dipole, so it radiates far less than the plasmon in Figure 1a. The localized plasmon modes are bunched together in a narrow range of wavelengths above where the real part of the dielectric function is below −2. The width of the peak is related to the imaginary part of the dielectric function, with silver tips having a much sharper peak than gold. This peak width is generally far wider than the separation of individual plasmon modes, so plasmon peaks are rarely resolved.

Figure 2b shows similar predictions, but for a mica substrate. There is almost no movement of the peak, being fixed at 533

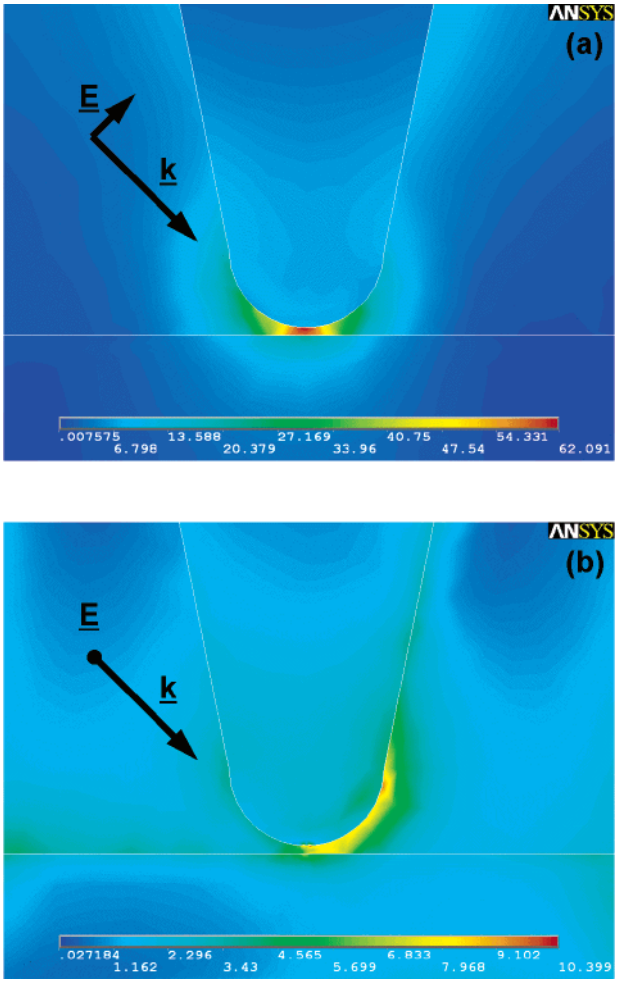

Figure 1. Finite element simulations of the enhancement of the electric field on the $y = 0$ plane, for a 20 nm radius gold tip 2 nm above a mica substrate, in air. The **k** vector of incidence is at 45° to the x (horizontal) and z (vertical) axes. (a) p-Polarization of the electric field (in the plane), which is used for the all the remaining simulations in this article. (b) s-Polarization of the electric field (out of the plane).

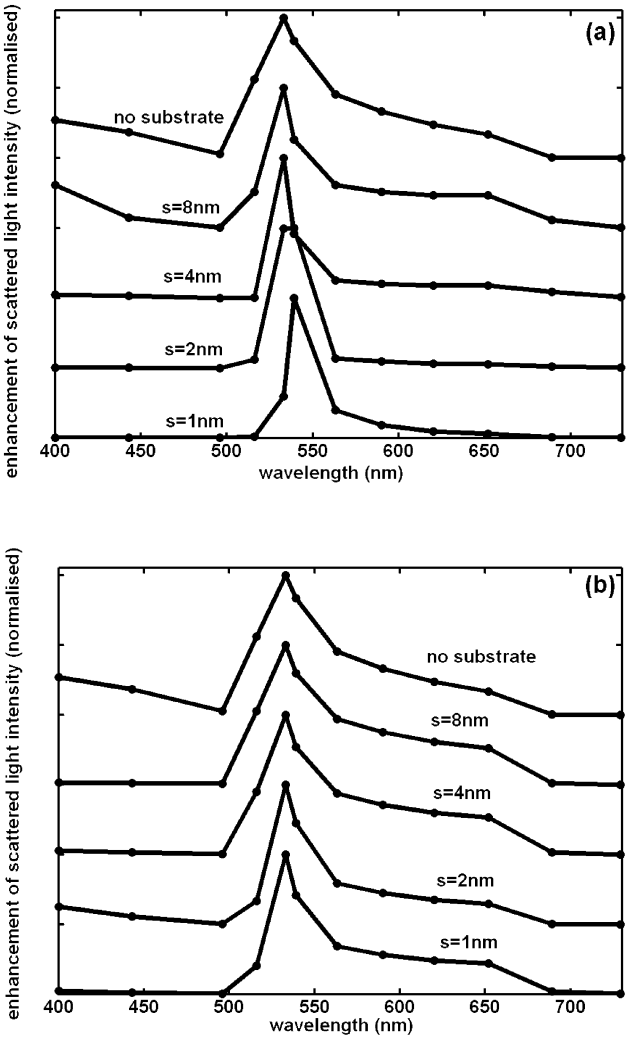

Figure 2. (a) Spectral dependence of the enhancement of the scattered light intensity (fourth power of electric field enhancement) for a 20 nm radius gold tip and a gold substrate, in air. A peak around the data point at 533 nm for large tip−substrate separation shifts toward the data point at 539 nm for small separation. (b) Curves for a 20 nm radius gold tip and a mica substrate. A peak around the data point at 533 nm is not shifted when the tip−substrate separation changes.

nm, which is very close in wavelength to the peak position in Figure 2a. This means that the gold tip dominates the form of the spectra. Mica, or any nonmetallic surface, is much more passive. Movement of the peak is reduced for a mica substrate compared to that for the gold substrates, as the plasmon modes move less. The intensity enhancement for mica substrates is also greatly reduced compared to gold. This is discussed later in more detail.

A silicon tip was modeled in Figure 3, as it has a low dielectric loss rate and is a common material for atomic force microscopy tips. With a silicon substrate, the overall enhancement is almost similar to that achievable for a gold tip and mica substrate. This is the best choice for studies in the near infrared range of the spectrum, giving an intensity enhancement higher than for a gold tip and gold substrate for wavelengths above 800 nm. This is particularly useful for biological samples, thanks to the reduced absorption of water in near-infrared region. Silicon dioxide in contrast is as passive as mica, acting like a spacer on top of the silicon. Silicon substrates and tips should have the minimum overlayer of oxide possible or the intensity of enhancement will be greatly reduced (although, the spectral form remains unchanged).

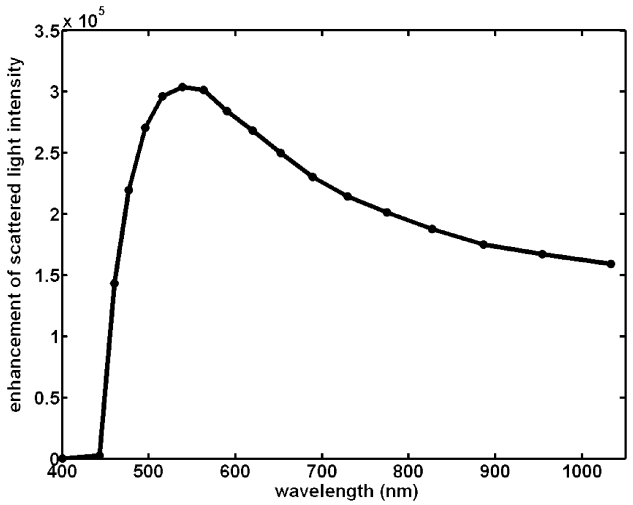

Figure 3. Spectral dependence of the enhancement of the scattered light intensity (fourth power of electric field enhancement) for a 20 nm radius silicon tip, 2 nm above a silicon substrate, in air. An unusually wide peak is observed, centered around 540 nm.

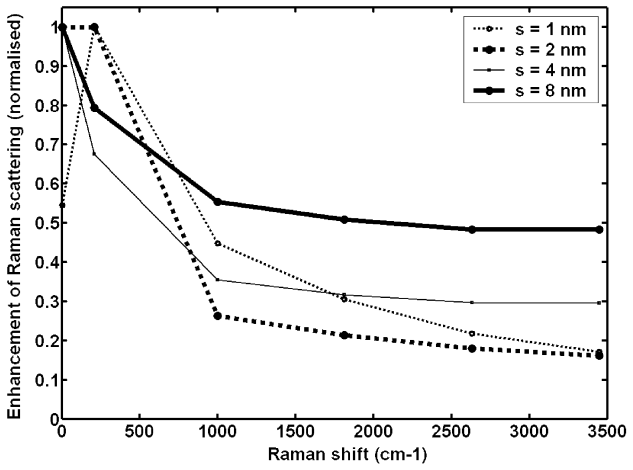

Figure 4. Spectral dependence of the enhancement of the Raman intensity, $(E_{elec}(\lambda_{inc}))^2 \cdot (E_{elec}(\lambda_{rad}))^2$ for an excitation of $\lambda_{inc} = 533$ nm and several λ_{rad} data points, for a gold tip of radius 20 nm, above a gold substrate in air. Spectra are repeated for various tip−substrate separations.

To model Raman spectroscopy, where incident and radiated wavelengths λ_{inc} and λ_{rad} are different, we plotted the spectral dependence of $(E_{elec}(\lambda_{inc}))^2 \cdot (E_{elec}(\lambda_{rad}))^2$ of a gold tip and gold substrate in Figure 4. The incident wavelength λ_{inc} was fixed at 533 nm, and a range of radiated wavelengths λ_{rad} were used: 533 nm (0 cm^{-1}), 539 nm (209 cm^{-1}), 563 nm (1000 cm^{-1}), 590 nm (1813 cm^{-1}), 620 nm (2633 cm^{-1}), and 652 nm (3448 cm^{-1}). The Raman spectrum is enhanced at low wavenumbers, because the excitation wavelength is close to the peak position in Figure 2a. At small separations $E_{elec}(\lambda_{rad})$ has a maximum in Figure 2 when λ_{rad} is 539 nm, so the peak in Figure 4 occurs at 539 nm (209 cm^{-1}). At larger separations, the maximum occurs when λ_{rad} is 533 nm. This demonstrates that a wide peak is better for uniformity of intensity of Raman spectra. However, this may not be too big an issue for spectroscopy, as one is generally interested in the wavenumber values of peak positions, not their relative intensities. For accurate Raman spectra, a reference sample such as aluminum is advised so that an unknown spectrum can be normalized to it. A silicon tip and substrate in Figure 3 give the most uniform peak, though intensity is reduced. Coating a silicon tip with 4 nm of gold

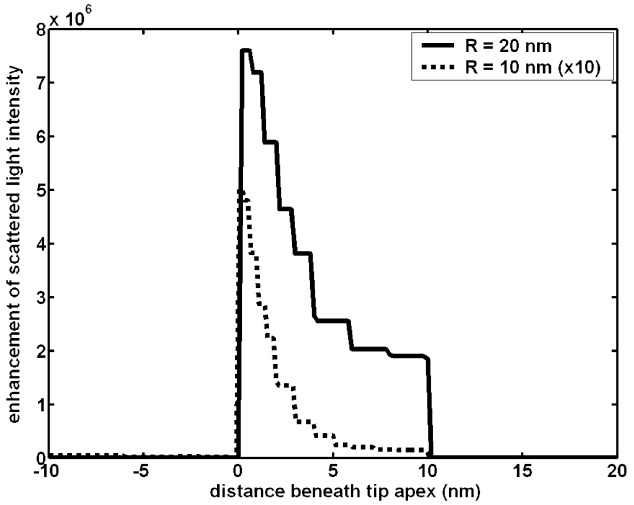

Figure 5. Dependence of the enhancement of the scattered light intensity (fourth power of electric field enhancement) on the position within the tip−substrate gap. The tip radius is 20 or 10 nm (enhancement × 10), the tip and substrate are gold, the tip−substrate separation is 10 nm, and the surrounding medium is air.

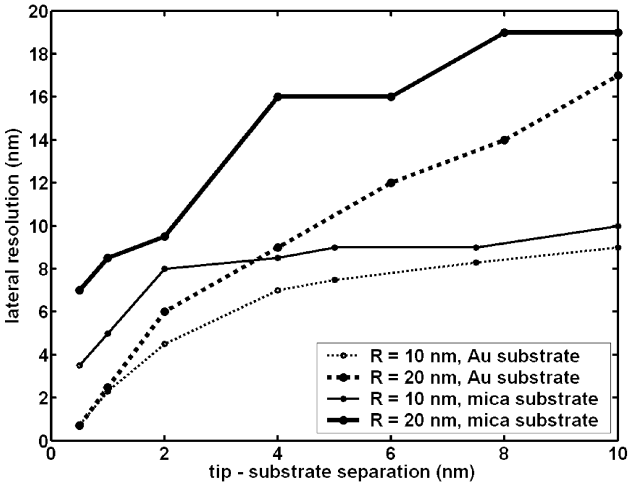

Figure 6. Lateral resolution in air of the enhancement of the scattered light intensity (fourth power of electric field enhancement) as a function of tip−substrate separation, on a constant *z* plane midway between the gold tip and substrate.

produces spectra very similar to that of pure gold tips, because the electric field dies away rapidly into the metal.

Although the spot beneath the tip in Figure 1a looks uniform, the fourth power of the electric field decays by 10% over the 2 nm between tip and substrate. When the separation increases to a size comparable to the tip radius, the exponential decay of the spot from tip to substrate is visible in Figure 5. The discrete jumps are due to the finite element size of the meshed model. It is clear that there is a far quicker decay for a tip radius of 10 nm than for one of 20 nm. The electric field decay can be closely approximated by the relation $\exp(-z/R)$, where z is the distance beneath the tip apex and R is the tip radius. This means that the scattered light intensity decays by the fourth power, or $\exp(-4z/R)$.

The lateral resolution is modeled in Figure 6. This lateral resolution is defined here as the full-width half-maximum of the Gaussian intensity enhancement on a plane midway between the tip and substrate. For gold substrates, the resolution can be approximated by the relation $\sqrt{(Rs)}$. STM light emission models suggest this resolution is approximately $\sqrt{(2Rs)}$.[24,25] However, STM light emission only has a radiative component, hence the

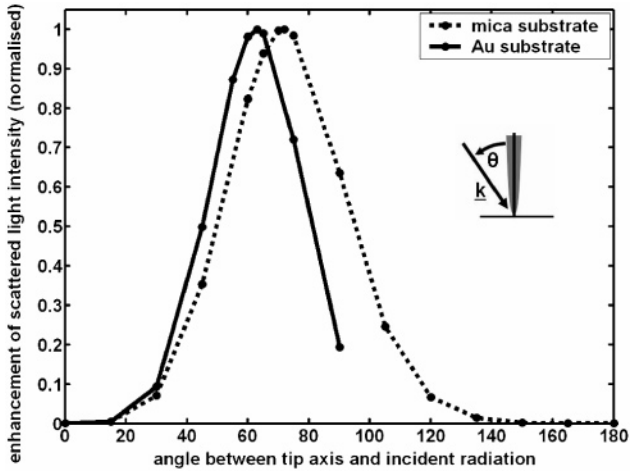

Figure 7. Angular dependence of the enhancement of the scattered light intensity (fourth power of electric field enhancement) for a 20 nm radius gold tip, 2 nm above a substrate of gold or mica, in air. Only the transparent mica substrate can excite the tip above 90°.

intensity is given by E^2 instead of the E^4 for this scattering process. This accounts for the factor of $\sqrt{2}$ in Gaussian widths between the two processes. At small values of tip−substrate separation, this relation is no longer observed. Indeed at a separation of 0.5 nm the achievable resolution is less than 1 nm. This was confirmed by re-meshing the model with several elements across the gap to ensure no meshing artifact existed. A similar molecular resolution has been observed in STM light emission[24] but not yet for apertureless microscopy. For large separation on mica substrates, the lateral resolution tends to a value approximated by the tip radius.

The angular dependence of illumination and radiation is shown in Figure 7 for gold and mica substrates illuminated at their spectral peak. As gold is opaque, angles above 90° (i.e. illumination from below) are not appropriate. The optimum angle for gold is 63°, whereas for mica this figure is 72°. For transparent samples, there is far less enhancement in the region where light can be collected (above about 120°). This means that an inverted microscope arrangement is not recommended, despite the smaller far-field spot size achievable.

As the tip radius increases, the enhancement intensity increases, due in part to a larger dipole volume. However, the greater than quadratic dependence for radii up to 20 nm gives way to a decline in enhancement for radii over 50 nm. This is most likely due to retardation effects, where parts of the dipole are sufficiently far apart for them to be no longer in phase.

We modeled the effect of a 2 nm thick layer of molecules on top of a gold or mica surface. The refractive index used was 1.46, which is that quoted for hydrogenated fats (i.e. saturated hydrocarbons). This gave rise to very little change in spectral features, but a reduction in the enhancement of intensity was observed.

Imaging under Water. A layer of water is adsorbed onto surfaces when scanning in air. The measured thickness on mica was reported as 0.2 nm at 50% relative humidity,[26] and on the Au(111) surface at 65% relative humidity it was also found to be 0.2 nm thick.[27] Although the simulations in air do not include a monolayer of water, this addition has a small modifying effect on the spectra.

Scanning probe microscopy is often performed in a totally aqueous (air free) environment in studies of biological samples. Relatively small quantities of ions may be added, but the liquid can be considered as pure water in terms of its optical properties.

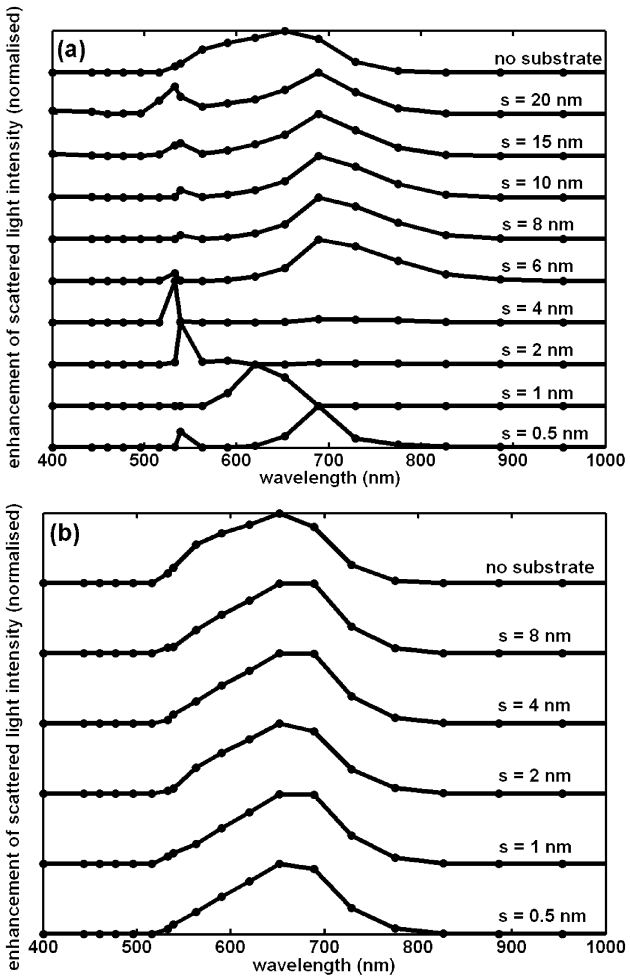

Figure 8. (a) Spectral dependence of the enhancement of the scattered light intensity (fourth power of electric field enhancement) for a 20 nm radius gold tip and a gold substrate in water. A peak around 533 nm is red-shifted at small separation, and another peak around 689 nm is more prevalent at larger separation. (b) Curves for a 20 nm radius gold tip and a mica substrate in water. A peak around 670 nm is insensitive to variations in tip−substrate separation.

When the air gap used in the simulations of Figure 2 is replaced by water, the results are surprisingly different. The single peak for gold surfaces is still present, but a second peak appears around 689 nm. At small separations, a geometric effect is visible—the plasmon modes are red-shifted as the tip−substrate separation decreases,[22] so the peak also shifts. At larger separations, the peak positions are more consistent. The 533 nm peak relates to the optical properties of the gold, but surprisingly it is not present in the spectra of Figure 8b. When a single sphere is immersed in water, the spectral peak position is affected by the environment.[28] The peak in Figure 8a moves from around 533 nm to where the real part of $\epsilon_{Au}(\lambda) = \epsilon_{water} \cdot \epsilon_{Au}$-(533 nm), where $\epsilon_{water} = 1.78$. This predicts a peak shift from 539 nm (where $\epsilon_{Au} = -6.3$) to about 670 nm (where $\epsilon_{Au} = -11.2$). So it seems that the tip 'sphere' is responsible for the red-shifted (~670 nm) peak, but the two-sphere localized plasmon (dominant for the Au substrate in Figure 8a) remains fixed at 533 nm. The movement of peaks for small separation is not ideal for imaging in water—the laser peak would have to be tuned to a wavelength somewhere between 533 and 689 nm. The tip−substrate separation would also have to be well maintained so that the spectral peak does not move, so any topographic variation would cause a substantial change in the intensity of scattered light. Furthermore, any variation of tip radius is equivalent to a variation in separation, hence tips would have to be produced with a very well-defined radius to minimize spectral shifts.

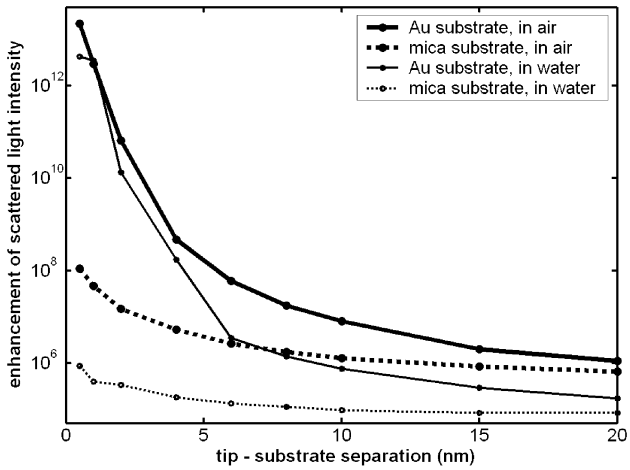

Figure 9. Dependence of the enhancement of the scattered light intensity (fourth power of electric field enhancement) on tip−substrate separation, for a 20 nm radius gold tip and a gold or mica substrate in air or water. The values are taken around the peak in the spectral response—533 nm in air, 652 nm for a gold substrate in water, and a variable wavelength for a gold substrate in water.

The spectra for a mica substrate (Figure 8b) displays lower peak mobility than the gold substrate in Figure 8a; it is therefore more stable for imaging. The peak position of about 670 nm compares well with the predicted shift for an isolated sphere when immersed in water.[28] For Raman and fluorescence spectroscopy, a laser of wavelength around 600 nm should be used for excitation, and emission would be measured in the range 600−750 nm.

The enhancement of the intensity for aqueous scanning is reduced compared to that in air, as can be seen from Figure 9. The figure shows extremely high enhancements (10^{12}) for Au substrates with small separation, whereas mica substrates' enhancement does not exceed 10^8. The decay of the intensity enhancement is stronger than exponential, with a decay length of about 0.5 nm per order of magnitude. This compares to the decay length of the tunnel current in scanning tunneling microscopy, which is around 0.1 nm. The short decay length is related to the very high lateral resolution observed in Figure 6. At very large separation, the tip behaves as if it is isolated, which leads to the intensity enhancements of around 10^5-10^6. Signal levels are discussed in detail below.

The lateral resolution under water is modeled in Figure 10, which is similar to those in air, except at small separation, where the ultimate resolution is not quite at the molecular level—limited to slightly less than 2 nm. Again, for large separation on mica substrates, the lateral resolution tends to a value approximated by the tip radius.

In air, the spot of enhancement is localized directly beneath the tip, whereas under water, the spot can be displaced laterally. This is visible in Figure 11, where the peaks are not symmetric or located directly under the tip apex. In both parts of the figure, values of $(E_{elec}(\lambda_{inc}))^2 \cdot (E_{elec}(\lambda_{rad}))^2$ were calculated for $\lambda_{inc} = 533$ nm and a variety of Raman-shifted wavelengths, λ_{rad}. Intensity changes as a function of wavenumber for a mica substrate (in Figure 11a) are similar to those in air seen in Figure 4. These intensity changes are even more dramatic for gold substrates. Simulations of 8 nm thick phospholipid bilayers ($n = 1.46$), on gold and mica substrates in water, give spectra similar to those without molecules, albeit with reduced intensity.

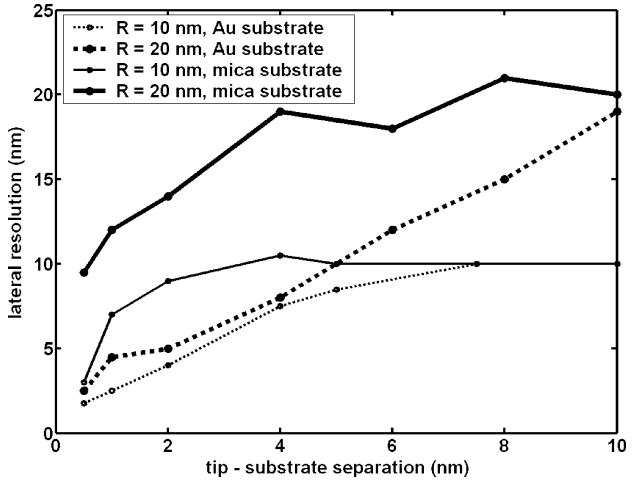

Figure 10. Lateral resolution in water of the enhancement of the scattered light intensity (fourth power of electric field enhancement) as a function of tip−substrate separation, on a constant *z* plane midway between the gold tip and substrate.

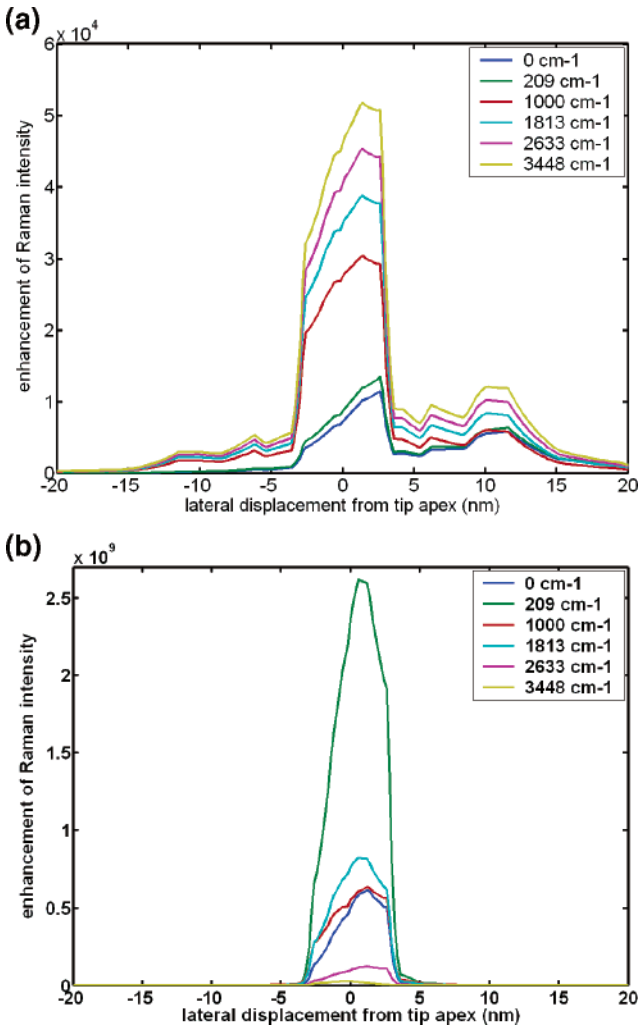

Figure 11. Values of the enhancement of the Raman intensity, $(E_{elec}(\lambda_{inc}))^2 \cdot (E_{elec}(\lambda_{rad}))^2$, on a constant *z* plane midway between the tip and substrate in water. The excitation wavelength is $\lambda_{inc} = 533$ nm, and curves for several values of λ_{rad} are displayed. (a) Curves for a gold tip and mica substrate in water. (b) Curves for a gold tip and gold substrate in water.

Discussion

A major result of these simulations is the molecular level lateral resolution predicted in Figure 6. This is achieved with a relatively large tip (10−20 nm radius), a size which can be produced in the laboratory by etching gold wires.[20]

However, a downside to molecular resolution is that the region from which the near-field signal originates is far smaller than the far-field illumination spot, limited in size by diffraction. Without any tip enhancement, the near-field signal would be dominated by the far-field signal. The diameter of the far-field spot will be about 0.6 λ/N.A. (N.A. = numerical aperture). For $\lambda = 600$ nm, and a long working distance lens with N.A. = 0.5, this gives a spot of around 700 nm in one axis and 700 nm/(sin 60°) = 1.4 μm for illumination at 60° in the other direction. The ratio of the near-field and far-field spots, *r*, is then 1 nm^2/(0.7 × 1.4) μm^2 = 10^{-6}.

Given that far-field Raman spectra can be acquired in around 1 s, with the order of kcps recorded for each peak, it is envisaged that the minimum proportion of near-field signal in the total signal must be above 10%. Otherwise the statistical noise in the far-field signal (the square root of the counts recorded) will be comparable to the near-field signal. In this case, subtracting the spectrum acquired for retracted tips from the spectrum of tips in close proximity will give the near-field signal plus a similar amount of noise. To achieve more than 10% near-field component in the total signal, the intensity enhancement must be at least $0.1/10^{-6} = 10^5$. Comparing this with the values of enhancement predicted from Figure 9, spectroscopy is readily achievable, with the exception of a mica substrate at large separation in water. These spectra can be acquired at each pixel in Raman mapping, though the long time taken to acquire each spectrum limits this to about 32 pixels.

A popular method of signal recovery in apertureless scanning near-field optical microscopy is to use lock-in amplification of the optical signal at a multiple of the frequency of tip oscillation. This removes the far-field signal by sampling the scattered light signal at the most nonlinear part of the tip oscillation, i.e. the last few nanometers. However, Raman signals are too small (with the order of 10^3 counts per second for a given Raman peak) to use lock-in techniques, due to the output current noise of detectors when pulses are not counted. Fluorescence signals, on the other hand, can be extracted at a multiple of the tip oscillation frequency as the signal strength is much greater than that of Raman.[29,30]

For large enhancements, the near-field spectrum can be larger than the far-field signal. To be able to acquire a whole spectrum in 10 ms, rather than 1 s, the ratio of near-field and far-field signals should be about 100. In this case, the enhancement must be at least $100/r = 10^8$. This high-speed spectral mapping is only possible for gold substrates and small separations ($s < 4$ nm), but it can be performed in water as well as air.

Conclusions

We have presented a finite element simulation of tip-enhanced Raman and fluorescence spectroscopy aimed at modeling realistic scanning conditions and materials. We varied a number of parameters to help impart an understanding of the process, including tip radius, tip material, substrate material, tip−substrate separation, wavelength, air or water environment, angle of illumination, and polarization. The enhancement of the electric field, E_{elec}, was measured under the tip apex which relates to the enhancement of the optical intensity as $E_{scat} = (E_{elec}(\lambda_{inc}))^2 \cdot (E_{elec}(\lambda_{rad}))^2$, λ_{inc} and λ_{rad} being the incident and radiated wavelengths, respectively. For elastic scattering, this reduces to the relation $E_{scat} = (E_{elec})^4$. This value was found to be as high as 10^{12} for a tip−substrate separation of 1 nm.

The lateral and vertical dependences of E_{elec} were also presented. The most notable result was that molecular resolution

imaging (<1 nm) is achievable, even with a relatively large radius tip (20 nm). We also made predictions for imaging in aqueous environments, noting a sizable red shift of the spectral peaks. Finally, we discussed signal levels, and predicted that high-speed Raman mapping should be possible with gold substrates and a small tip−substrate separation (<4 nm).

Acknowledgment. This work was supported by an award from The Medical Research Council. We thank Ioan Notingher for helpful discussions.

References and Notes

(1) In certain cases, especially at low temperature, electronic surface states can be resolved which relate to the 'd' electrons and therefore chemical identity. Li, J.; Schneider, W.-D.; Berndt, R. *Phys. Rev. B* **1997**, *56*, 7656. Jamneala, T.; Madhavan, V.; Chen, W.; Crommie, M. F. *Phys. Rev. B* **2000**, *61*, 9990.

(2) Pohl, D.; Fischer, U.; Durig, U. *J. Microsc.* **1988**, *152*, 853.

(3) Zenhausern, F.; Martin, Y.; Wickramasinghe, H. K. *Science* **1995**, *269*, 1083.

(4) Hillenbrand, R.; Keilmann, F. *Phys. Rev. Lett.* **2000**, *85*, 3029.

(5) Pettinger, B.; Ren, B.; Picardi, G.; Schuster, R.; Ertl, G. *J. Raman Spectrosc.* **2005**, *36*, 541.

(6) Stockle, R.; Suh, Y.; Deckert, V.; Zenobi, R. *Chem. Phys. Lett.* **2000**, *318*, 131.

(7) Hayazawa, N.; Yano, T.; Watanabe, H.; Inouye, Y.; Kawata, S. *Chem. Phys. Lett.* **2003**, *376*, 174.

(8) Hayazawa, N.; Inouye, Y.; Sekhat, Z.; Kawata, S. *J. Chem. Phys.* **2002**, *117*, 1296.

(9) McCall, S. L.; Platzman, P. M. *Phys. Rev. B* **1980**, *22*, 1660.

(10) Anderson, N.; Hartschuh, A.; Cronin, S.; Novotny, L. *J. Am. Chem. Soc.* **2005**, *127*, 2533.

(11) Nie, S.; Emory, S. *Science* **1997**, *275*, 1102.

(12) Kneipp, K.; Wang, Y.; Kneipp, H.; Perelman, L.; Itzkan, I.; Dasari, R.; Feld, M. *Phys. Rev. Lett.* **1997**, *78*, 1667.

(13) Gerton, J.; Wade, L.; Lessard, G.; Ma, Z.; Quake, S. *Phys. Rev. Lett.* **2004**, *93*, 180801.

(14) Novotny, L.; Bian, R.; Xie, X. *Phys. Rev. Lett.* **1997**, *79*, 645.

(15) Martin, Y.; Hamann, H.; Wickramasinghe, H. J. *Appl. Phys*. **2001**, *89*, 5774.

(16) Geshev, P.; Klein, S.; Witting, T.; Dickmann, K.; Hietschold, M. *Phys. Rev. B* **2004**, *70*, 075402.

(17) Milner, R.; Richards, D. *J. Microsc*. **2001**, *202*, 66.

(18) Notingher, I.; Elfick, A. *J. Phys. Chem. B* **2005**, *109*, 15699.

(19) Micic, M.; Klymyshyn, N.; Suh, Y.; Lu, H. *J. Phys. Chem. B* **2003**, *107*, 1574.

(20) Billot, L.; Berguiga, L.; de la Chapelle, M. L.; Gilbert, Y.; Bachelot, R. *Eur. Phys. J. Appl. Phys.* **2005**, *31*, 139.

(21) Weaver, J.; Frederikse, H. In *CRC Handbook of Chemistry and Physics*; Lide, D., Ed.; CRC Press: Boca Raton, FL, 1995; Sec. 12, p 126.

(22) Downes, A.; Taylor, M.; Welland, M. *Phys. Rev. B* **1998**, *57*, 6706.

(23) Johansson, P.; Monreal, R.; Apell, P. *Phys. Rev. B* **1990**, *42*, 9210.

(24) Downes, A.; Welland, M. *Phys. Rev. Lett.* **1998**, *81*, 1857.

(25) Rendell, R. W.; Scalapino, D. *J. Phys. Rev. B* **1981**, *24*, 3276.

(26) Beaglehole, D.; Radlinska, E. Z.; Ninham, B. W.; Christenson, H. K. *Phys. Rev. Lett.* **1991**, *66*, 2084.

(27) Gil, A.; Colchero, J.; Luna, M.; Gómez-Herrero, J.; Baró, A. M. *Langmuir* **2000**, *16*, 5086.

(28) Swanson, N. L.; Billard, B. D. *Nanotechnology* **2003**, *14*, 353.

(29) Fragola, A.; Aigouy, L.; De Wilde, Y.; Mortier, M. *J. Microsc.* **2003**, *210*, 198.

(30) Hillenbrand, R.; Keilmann, F. *Appl. Phys. Lett.* **2002**, *80*, 25.